5th IFAC Symposium on Mechatronic Systems
Marriott Boston Cambridge
Cambridge, MA, USA, Sept 13-15, 2010

Synthesis of Stable Grasp by Four-Fingered Robot Hand for Pick-and-Place of Assembling Parts

Akira Nakashima * **Takashi Uno** * **Yoshikazu Hayakawa** *,**
Toshiyuki Kondo *** **Shinji Sawada** *** **Nobuhiro Nanba** ***

* *Mechanical Science and Engineering, Graduate School of Engineering, Nagoya University, Furo-cho, Chikusa-ku, Nagoya, Japan (e-mail: a_nakashima@nuem.nagoya-u.ac.jp)*
** *RIKEN-TRI Collaboration Center, RIKEN, 2271-103, Anagahora, Shimoshidami, Moriyama-ku, Nagoya, Japan.*
*** *Honda Engineering Co. Ltd., 6-1, Hagadai, Hagamachi, Hagagun, Tochigi, Japan*

Abstract: This paper proposes a synthesis methodology of stable grasp by a four-fingered robot hand in order to automate preparation for assembling work, which is composed of recognition, grasp and carry of assembling parts. An optimization method of grasping forces, object configuration and contact points is proposed. The criterion of the optimization is appropriate normalized distances from the planes of a constraint polyhedron, which is derived by the friction and joint torque limitations. An experimental result of grasp of a door mirror is shown to verify the effectiveness of the proposed method.

Keywords: handling, robot control, stability criteria, industrial robots, optimization problems

1. INTRODUCTION

There are press, welding, painting and *assembling* work in process of operation of product line for automobiles as shown in Fig. 1. The assembling work is carried out by humans because of its complicacy while the first three works have been automated by robot manipulators in the product lines. The automation of the assembling work can reduce manufacturing cost and improve work environment. The work to fix a door mirror to a door as an example of the assembling work is illustrated in the box of Fig. 1. The process of the operation is composed of the preparation for the fixing and the fixing of the mirror. The preparation includes the recognition, grasp, carry of the mirror. Humans use their own eyes, arms, hands and machine tools in the assembling work. It is complex and difficult for robot arms to use the machine

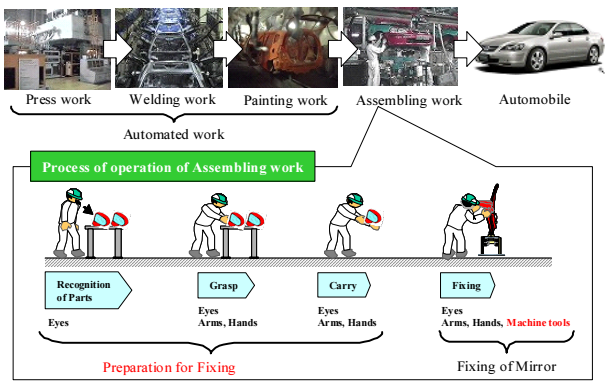

Fig. 1. Product line of automobiles.

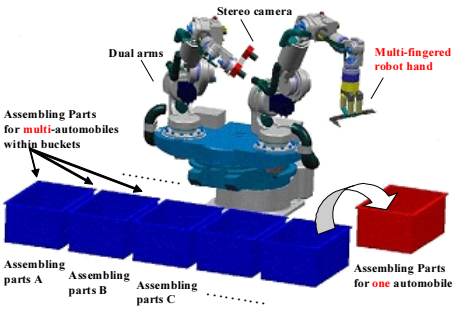

Fig. 2. Two-arms system for automating the preparation.

tools in the fixing. On the other hand, the machine tools are not necessary and the eyes, arms and hands can be alternated with vision-cameras, robot arms and robot hands. Therefore, as the first step of the automation of the assembling work, we aim to automate the preparation for assembly by a two-arms system as shown in Fig. 2. It is assumed that the assembling parts of multi-automobiles are contained in the each blue bucket. The stereo camera of the left arm detects the shapes and position/orientation of the parts in the buckets. The multi-fingered robot hand of the right arm grasps the parts with the detected information and collects the parts for one automobile up in the red bucket. This system thus can devote humans to carry out only the assembling work.

In this paper, we concentrate on grasp by a multi-fingered robot hand. A multi-fingered robot hand allows a robot arm to grasp a large class of objects with a single end-effector because the hand can grasp with multi contacts and can control grasping forces via multi joint inputs. It is

an important issue to find the set of the contact points for the grasping forces to be balanced with the gravity force. Investigation methods of the contact points have been proposed by Omata (1990, 1993); Trinkle and Paul (1990); Li et al. (2002). It is also another important issue to determine the grasping forces with criteria since the grasping forces have the redundancy, i.e., the *internal force* (Salisbury and Roth (1983)). Kerr and Roth (1986) proposed an optimization method for the grasping forces with respect to the distances from the planes of a constraint polyhedron derived from the friction and joint torque limitations. Nakamura et al. (1989) considered a safety factor which means that the small grasping force is better with being included in the frictional domain. Yoshikawa and Nagai (1991) proposed a decomposition of the grasping forces to manipulating and grasping forces with compatible physical meaning. Nguyen (1988) considered an investigation method of the contact points to achieve the *force-closure*. The force-closure is the ability for the grasping forces to resist any external disturbances to the grasped object and is a major criterion for the grasp stability. Li and Sastry (1988) proposed the criterion where the disturbance force and moment is evaluated by the volume of the ellipsoid derived from the singular value decomposition of the grasp map. Markenscoff and Papadimitriou (1989) investigated the set of the contact points minimizing the grasping forces with any normalized disturbance forces. Magialardi et al. (1996) derived the set of the contact points minimizing the grasping forces by considering the disturbance force and moment in a sequential order. Watanabe and Yoshikawa (2003b) optimized the set of the contact points minimizing the grasping forces with a required external force set which is an extended criterion of any disturbance forces. The force limitation and the object region with respect to the fingers have been not considered in these studies. Watanabe and Yoshikawa (2003a) extended their previous problem to the one with required acceleration of the object and considered the force limitation and the object region.

The methods and algorithms in the mentioned studies are not feasible in two points of view of the optimization criterion and the finger configuration. The vector norm of the grasping forces is minimized in the studies of the force-closure while Watanabe and Yoshikawa (2003b) minimized the vector norm of one grasping force which is the maximum in all the grasping forces. On the other hand, Kerr and Roth (1986) maximized the minimum of the distances of the grasping forces from the planes of the constraint polyhedron. The planes represent the bounds derived from the friction and torque limitations. The criterion of the distances can be better than the vector norm of the grasping forces because the former criterion denotes the safety factor not to break the contacts. However, in the study of Kerr and Roth (1986), since the distances from the planes are not normalized to appropriate scales, the optimized grasping forces can be close to some of the bounds. We consider the distances normalized by the norms of the normal vectors of the planes. Watanabe and Yoshikawa (2003a) considered the region of the position and orientation of the object with respect to the fingers. However, they did not show a method to obtain the object region, which depends on the finger configuration and angle limitation. We show a method to derive the object region with respect to a four-fingered robot hand.

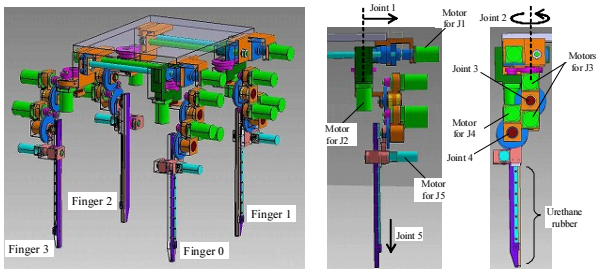

(a) An overview of the four-fingered robot hand (b) The configuration of the joints and motors

Fig. 3. The four-fingered robot hand.

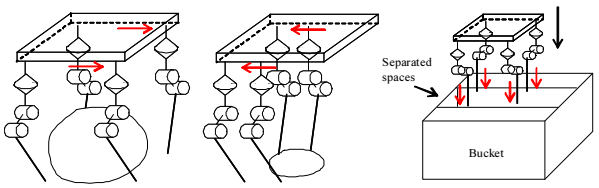

(a) Grasp of a large object (b) Grasp of a small object (c) Adjustment for narrow spaces

Fig. 4. The adjustment of the hand.

2. SYSTEM AND BASIC ANALYSES

2.1 Four-Fingered Robot Hand

The four-fingered robot hand for grasping assembling parts is shown in Fig. 3 where the fingers are numbered by $i = 0, \cdots, 3$ as the figure (a). The finger 0 is shown in the figure (b) where the 1st and 5th joints are prismatic and the 2nd, 3rd, 4th joints are rotational. The other fingers are the same as the finger 0 expect for the 1st joints and the fingers 2 and 3 do not has the 1st prismatic joint. The 1st and 2nd joints are driven by a ball screw (the pitch of 1 [mm]) and a rack and pinion gear (the gear ratio of 1:4). The gear ratios of the 2nd–4th joints are 1:2, 1:4 and 1:4 respectively and note that the joint 3 is driven by the two motors. The motors of the 1st–4th joints and the 5th joint are the AC servo actuators of RSF-5A and RSF-3A (Harmonic Drive Systems, Inc.). The maximum torques of the joints are 1.4 and 0.3 [Nm] respectively. Urethane rubbers are bonded on the surfaces of the 5th links for the grasp. The hand can adjust the configuration to both small and large objects by changing the 1st joints of the fingers 0 and 1 as in Fig. 4 (a) and (b). The hand can also adjust the lengths of the 5th links to separated narrow spaces by the 5th joints. The 2nd, 3rd and 4th joints are used for controlling the grasping forces.

The frame configuration is illustrated in Fig. 5. Σ_h is the reference frame and Σ_{i0} is the base frame of the finger i.

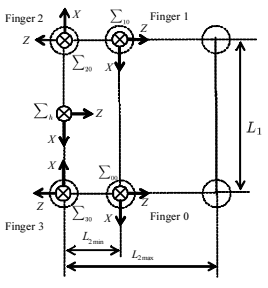

Fig. 5. The frame configuration of the hand.

The frame configurations of all the fingers are the same except for the 5th frames. The X_5-axes are outside and parallel to the long sides of the 5th frames. The Z_5-axes are opposite each other in the cases of $i = 0, 2$ and $i = 1, 3$ in order for the Z_5-axes to be outside and normal to the urethane rubbers. $L_1 = 176$ [mm] is the distance between the fingers 0 and 1 and $L_{2\min} = 48$ and $L_{2\max} = 158$ [mm] are the minimum and maximum distances between the fingers 0 and 3. Figure 6 shows the frame configuration of the fingers. The link parameters are $Z_{12} = 62$, $X_{34} = 61.5$, $Y_{34} = 24$ $(i = 0, 2), -24$ $(i = 1, 3)$, $X_{45} = 220$, $Y_{45} = -24$ $(i = 0, 2), 24$ $(i = 1, 3)$ and $Z_{45} = -13.9$ [mm]. The links depicted by the dotted lines represent the cases of the finger 1 and 3. The joints are represented by q_{i1}, q_{i5} [mm] and q_{i2}–q_{i4} [rad]. The positions of the centers of mass of the 3rd–5th links are $(X_{3c}, Y_{3c}) = (22, 10.5)$ $(i = 0, 2)$, $(22, -10.5)$ $(i = 1, 3)$, $(X_{4c}, Y_{4c}) = (29.7, 5.9)$ $(i = 0, 2)$, $(29.7, -5.9)$ $(i = 1, 3)$ and $X_{5c} = -124$ [mm] expressed in the 3rd–5th frames. The mass of the 3rd–5th links are $m_3 = 0.408$, $m_4 = 0.073$ and $m_5 = 0.081$ [kg]. The joint limitations are $0 \le q_{i5} \le 110$ [mm] $(i = 0, 1)$, $-26 \le q_{i2} \le 90$ $(i = 0, 2)$, $-90 \le q_{i2} \le 26$ $(i = 1, 3)$, $-94 \le q_{i4} \le 139$ $(i = 0, 2)$, $-139 \le q_{i4} \le 94$ $(i = 1, 3)$ [deg] and $-54 \le q_{i5} \le 0$ [mm]. Furthermore, the sum of q_{i3} and q_{i4} is bounded as $|q_{i3} + q_{i4}| \le \frac{\pi}{2}$.

2.2 Kinematic and Force Analyses

In the latter, the script i is dropped for notation simplicity if it is not necessary. The forward kinematics is firstly shown. The position of the 5th frame with respect to the base frame Σ_0 is given by

$$\begin{aligned} p_x &= \bar{q}_5 c_2 s_{34} + Y_{45} c_2 c_{34} + Z_{45} s_2 + c_2(X_{34} s_3 + Y_{34} c_3) \\ p_y &= \bar{q}_5 c_{34} - Y_{45} s_{34} + X_{34} c_3 - Y_{34} s_3 + Z_{12} \\ p_z &= \bar{q}_5 s_2 s_{34} + Y_{45} s_2 c_{34} - Z_{45} c_2 + s_2(X_{34} s_3 + Y_{34} c_3) + q_1, \end{aligned} \tag{1}$$

where $\bar{q}_5 := X_{45} + q_5$, $s_2 := \sin q_2$, $c_2 := \cos q_2$, $s_{34} := \sin(q_3 + q_4)$ and $c_{34} := \cos(q_3 + q_4)$.

The inverse kinematics is secondly analyzed. The contact points and the corresponding normal vectors on the object are assumed to be given. Since the contact surfaces of the fingers are soft and flat, it necessary to satisfy the following constraints:

$$\boldsymbol{X}_5^{\mathrm{T}} \boldsymbol{n} = 0, \ \boldsymbol{Z}_5^{\mathrm{T}} \boldsymbol{n} \le \cos\bar{\theta} \tag{2}$$

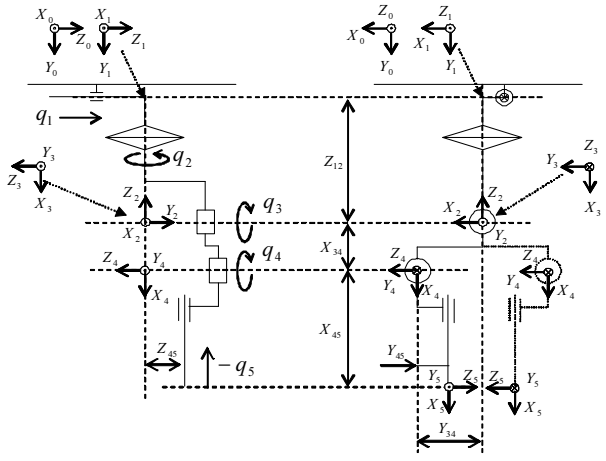

Fig. 6. The frame configuration of the finger.

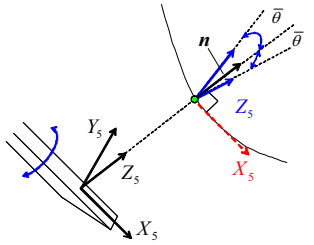

Fig. 7. The finger joint constraints.

where

$$\boldsymbol{X}_5 := \begin{bmatrix} c_2 s_{34} \\ c_{34} \\ s_2 s_{34} \end{bmatrix}, \ \boldsymbol{Z}_5 := -\begin{bmatrix} c_2 c_{34} \\ -s_{34} \\ s_2 c_{34} \end{bmatrix} (i = 0, 2), \begin{bmatrix} c_2 c_{34} \\ -s_{34} \\ s_2 c_{34} \end{bmatrix} (i = 1, 3).$$

$\boldsymbol{X}_5, \boldsymbol{Z}_5 \in \mathbb{R}^3$ are the vectors in the X_5, Z_5-axes and $\boldsymbol{n} \in \mathbb{R}^3$ is the normal vector at the contact point. The constraints (2) is illustrated in Fig. 7. The first of (2) denotes that the long side of the urethane rubber is normal to the surface. The second of (2) denotes that the angle between the narrow side and the surface is allowed within $\bar{\theta}$ because the urethane can be deformed and adapted on the surface despite the difference $\bar{\theta}$. The joint ranges to satisfy (2) is given by the following theorem:

Theorem 1. Suppose $|q_3 + q_4| \le \frac{\pi}{2}$, $|\bar{\theta}| < \frac{\pi}{2}$ and $|n_y| \le \cos\bar{\theta}$. Then, the constraints of (2) are solved as

$$q_3 + q_4 = Q_{34}(q_2), \ Q_{34} := \begin{cases} (\pi - \phi_{34})\mathrm{sgn}(\phi_{34}) & (i = 0, 2) \\ -\phi_{34} & (i = 1, 3) \end{cases} \tag{3}$$

$$\begin{cases} -\pi + \sin^{-1} l_2 - \phi_2 \le q_2 \le -\sin^{-1} l_2 - \phi_2 & (i = 0, 2) \\ \sin^{-1} l_2 - \phi_2 \le q_2 \le \pi - \sin^{-1} l_2 - \phi_2 & (i = 1, 3) \end{cases} \tag{4}$$

where

$$\phi_2 := \mathrm{atan2}(n_x, n_{nz}), \ l_2 := \sqrt{(\cos^2\bar{\theta} - n_y^2)/(n_x^2 + n_z^2)}$$
$$\phi_{34}(q_2) := \mathrm{atan2}(n_y, n_x \cos q_2 + n_z \sin q_2).$$

Proof . The first of (2) is calculated as

$$\boldsymbol{X}_5^{\mathrm{T}} \boldsymbol{n} = \sqrt{(n_x \cos q_2 + n_z \sin q_2)^2 + n_y^2} \sin(q_3 + q_4 + \phi_{34}) = 0. \tag{5}$$

Eq. (5) leads to

$$q_3 + q_4 = m\pi - \phi_{34} \ (m = 0, \pm 1, \pm 2, \cdots) \tag{6}$$

The second of (2) is calculated by (6) and $\cos\bar{\theta} > 0$ as

$$\boldsymbol{Z}_5^{\mathrm{T}} \boldsymbol{n} = \sqrt{(n_x \cos q_2 + n_z \sin q_2)^2 + n_y^2} \ge \cos\bar{\theta} \tag{7}$$

$$\begin{cases} \cos(q_3 + q_4 + \phi_{34}) = -1 & (i = 0, 2) \\ \cos(q_3 + q_4 + \phi_{34}) = 1 & (i = 1, 3) \end{cases}. \tag{8}$$

Considering (8) and $|q_3 + q_4| \le \frac{\pi}{2}$ yields to $m = 1$ $(\phi_{34} > 0)$, $m = -1$ $(\phi_{34} < 0)$ $(i = 0, 2)$ and $m = 0$ $(i = 1, 3)$. This result and (6) lead to (3). (7) is rewritten using $|n_y| \le \cos\bar{\theta}$ as

$$\left([n_x \ n_z][c_2 \ s_2]^{\mathrm{T}}\right)^2 \ge \cos^2\bar{\theta} - n_y^2 \ge 0 \tag{9}$$

Note that $[c_2 \ s_2]^{\mathrm{T}}$ represents the direction of X_2-axis of the 2nd frame in (X, Y)-plane. Since the X_2-axis is opposite to $(i = 0, 2)$ or same as $(i = 1, 3)$ the X_5-axis of the 5th frame in (X, Y)-plane from the definition of the frame configuration (See Fig. 6), the inner product between $[n_x \ n_z]^{\mathrm{T}}$ and $[c_2 \ s_2]^{\mathrm{T}}$ is negative $(i = 0, 2)$ or positive $(i = 1, 3)$. Therefore, (9) is considered as

$$\sin(q_2+\phi_2) \le -l_2 \ (i=0,2), \ \ \sin(q_2+\phi_2) \ge l_2 \ (i=1,3). \tag{10}$$

(4) can be easily obtained by solving (10). ∎

The joint angles for the origin the 5th frame to contact on a desired point on the object is given by the theorem:

Theorem 2. Suppose that q_1 is a constant of q_1^*, a desired contact point (p_x, p_y, p_z) is given and Theorem 1. Then, the solutions q_2^*–q_5^* of (1) are given by

$$q_2^* = \cos^{-1}\left(\frac{Z_{45}}{\sqrt{p_x^2+(p_z-q_1^*)^2}}\right) + \psi_2^* \tag{11}$$

$$q_3^* = \cos^{-1}\left(\frac{l_3^*}{\sqrt{(X_{34}+Y_{34}t_{34}^*)^2+(Y_{34}-X_{34}t_{34}^*)^2}}\right) + \psi_3^* \tag{12}$$

$$q_4^* = Q_{34}(q_2^*) - q_3^* \tag{13}$$

$$q_5^* = (p_y + Y_{45}s_{34}^* - X_{34}c_3^* + Y_{34}s_3^* - Z_{12})/c_{34}^* - X_{45} \tag{14}$$

where $t_{34} := \tan(q_3+q_4)$ and

$\psi_2^* := \mathrm{atan2}(p_x, q_1^* - p_z)$

$l_3^* := p_x c_2^* + (p_z - q_1^*)s_2^* - Y_{45}c_{34} - t_{34}^*(p_y + Y_{45}s_{34}^* - Z_{12})$

$\psi_3^* := \mathrm{atan2}(X_{34}+Y_{34}t_{34}^*, Y_{34} - X_{34}t_{34}^*)$.

Proof . Eqs. (1) is rewritten in the following matrix form:

$$\begin{bmatrix} p_x \\ p_z - q_1^* \end{bmatrix} = \begin{bmatrix} c_2 & s_2 \\ s_2 & -c_2 \end{bmatrix} \begin{bmatrix} Y_{45}c_{34} + X_{45}s_{34} + X_{34}s_3 + Y_{34}c_3 \\ Z_{45} \end{bmatrix}$$

$$\Leftrightarrow \begin{bmatrix} Y_{45}c_{34} + X_{45}s_{34} + X_{34}s_3 + Y_{34}c_3 \\ Z_{45} \end{bmatrix} = \begin{bmatrix} c_2 & s_2 \\ s_2 & -c_2 \end{bmatrix} \begin{bmatrix} p_x \\ p_z - q_1^* \end{bmatrix} \tag{15}$$

The second equation of (15) is transformed to

$$\cos(q_2 - \psi_2) = \frac{Z_{45}}{\sqrt{p_x^2+(p_z-q_1^*)^2}}. \tag{16}$$

(16) leads to (11). Substituting q_2^* into the first equation of (15) and (1) and combining the resultant equations with respect to $(X_{45}+q_5)$ yield

$$(X_{34}+Y_{34}t_{34}^*)s_3 + (Y_{34} - X_{34}t_{34}^*)c_3 = l_3^*. \tag{17}$$

(17) leads to (12). (13) is given by q_2^*, q_3^*, $Q_{34}(q_2^*)$ of (3). (14) can be easily obtained by q_2^*, q_3^*, $Q_{34}(q_2^*)$ and (1). ∎

Example 1. Figure 8 shows an example of the grasp of a door mirror. The figure (a) is the discrete data on the mirror plotted by the blue dots. The green circles and the red arrows represent the contact points and the normal vectors. The mirror frame Σ_m is attached to the center of mass. The contact points and the normal vectors in figure (a) are expressed in Σ_m as

$$\boldsymbol{p}_A = \begin{bmatrix} 69 \\ -21 \\ 27 \end{bmatrix}, \ \boldsymbol{p}_B = \begin{bmatrix} -67 \\ -21 \\ 26 \end{bmatrix}, \ \boldsymbol{p}_C = \begin{bmatrix} -69 \\ -21 \\ -33 \end{bmatrix}, \ \boldsymbol{p}_D = \begin{bmatrix} 59 \\ -21 \\ -45 \end{bmatrix}$$

$$\boldsymbol{n}_A = \begin{bmatrix} -0.94 \\ 0.19 \\ 0.29 \end{bmatrix}, \boldsymbol{n}_B = \begin{bmatrix} 0.95 \\ 0.28 \\ 0.17 \end{bmatrix}, \boldsymbol{n}_C = \begin{bmatrix} 0.92 \\ 0.16 \\ 0.37 \end{bmatrix}, \boldsymbol{n}_D = \begin{bmatrix} -0.83 \\ 0.04 \\ 0.55 \end{bmatrix}.$$

The figure (b) shows the configuration of the hand and the mirror. The axes of (X_h, Y_h, Z_h) coincides with the axes of (Z_m, Y_m, X_m). Figure 9 shows the reachable areas of the fingers in the case of $q_{11} = q_{21} = 0$. The black areas are the reachable areas in the (X_m, Z_m)-plane ((X_h, Z_h)-plane). The red circle is the origin of Σ_h, the green circles is the contact positions and the position of the center of mass is $(5, -35)$ [mm]. It is confirmed that all the contact points

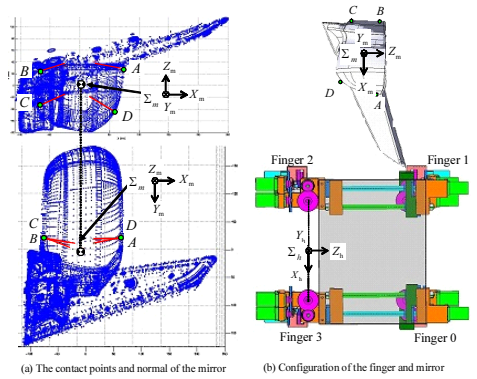

Fig. 8. An example of the grasp of a door mirror.

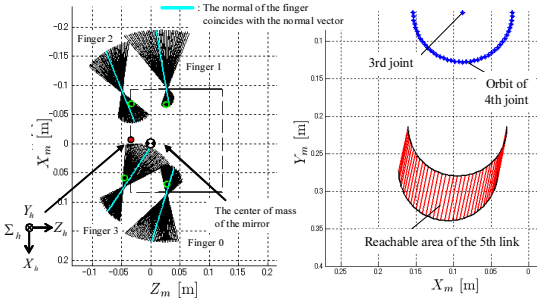

Fig. 9. The reachable area of the fingers.

are included in the reachable area. The aqua lines mean that the normals of the finger coincide with the contact normal. It is expected that the hand can easier grasp the mirror by adjusting the relative configuration between the hand and the mirror in order for the contact points to be close to the aqua lines. The red area in the left figure is the reachable area of the 5th link. The distance of the contact points from the hand in the Y_h-axis should be middle within the red area.

The static force is finally analyzed. The joint torque is defined as $\boldsymbol{\tau} := [\tau_2 \ \tau_3 \ \tau_4 \ \tau_5]^{\mathrm{T}} \in \mathbb{R}^4$. The grasping force $\boldsymbol{f} \in \mathbb{R}^3$ is expressed as $\boldsymbol{f} = f\boldsymbol{n}_f$, where f is the magnitude and $\boldsymbol{n}_f \in \mathbb{R}^3$ is the normalized direction. The static relation between $\boldsymbol{\tau}$ and $\boldsymbol{f}$ is given by

$$\boldsymbol{\tau} = \boldsymbol{J}(\boldsymbol{q})^{\mathrm{T}}\boldsymbol{f}, \tag{18}$$

where $\boldsymbol{J} \in \mathbb{R}^{3\times 5}$ is the jacobian matrix defined as $\boldsymbol{J} := (\partial \boldsymbol{p}/\partial \boldsymbol{q})^{\mathrm{T}}$ with $\boldsymbol{p} := [p_x \ p_y \ p_z]^{\mathrm{T}}$ and (1). Let us consider the maximum of the grasping force $f_{\max}$ when $\boldsymbol{n}_f$ is given. $f_{\max}$ is given by the following theorem:

Theorem 3. Suppose that the direction of the force $\boldsymbol{n}_f$ and the maximum values of the torque $\tau_{i\max}$ are given. Then, $f_{\max}$ is solved as

$$f_{\max} = \min_i |\tau_{i\max}/u_i|, \tag{19}$$

where u_i is the component of

$$\boldsymbol{u} := \boldsymbol{J}^{\mathrm{T}}\boldsymbol{n}_f \tag{20}$$

Proof . Combining $\boldsymbol{f} = f\boldsymbol{n}_f$, (18) and (20) leads to

$$\tau_i = u_i f. \tag{21}$$

Substituting (21) into $|\tau_i| \le \tau_{i\max}$ results in

$$|f| \le |\tau_{i\max}/u_i|. \tag{22}$$

Therefore, $f_{\max}$ is given by the minimum of $|\tau_{i\max}/u_i|$. ∎

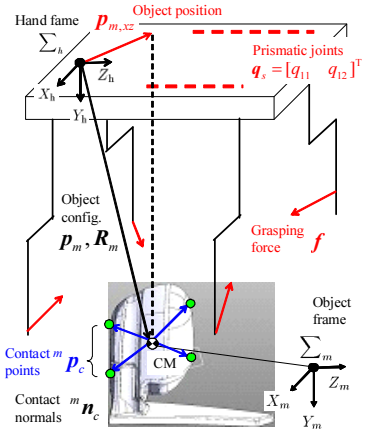

Fig. 10. The configuration of the grasp optimization.

Theorem 3 is necessary for the calculation of the distances of the grasping forces from the constraint bounds of the torque limitation.

3. GRASP OPTIMIZATION

3.1 Problem Setting

Figure 10 illustrates the variables and parameters in the grasp optimization. $\boldsymbol{p}_m \in \mathbb{R}^3$ and $\boldsymbol{R}_m \in \mathbb{R}^{3\times3}$ are the position vector and the rotation matrix of the object frame Σ_m. The contact point expressed in Σ_h is related to the one in Σ_m as

$$\boldsymbol{p}_{c_i} = \boldsymbol{p}_m + \boldsymbol{R}_m {}^m\boldsymbol{p}_{c_i}, \tag{23}$$

where ${}^m\boldsymbol{p}_{c_i} \in \mathbb{R}^3$ is the ith contact point expressed in Σ_m. In the latter, position vectors without any left superscripts are expressed inΣ_h. Suppose that the contact normals ${}^m\boldsymbol{n}_c \in \mathbb{R}^{12}$, the y-position and orientation of the object, i.e., $p_{m,y}$ and $\boldsymbol{R}_m$ are given. are given. The grasp is optimized with respect to the grasping forces $\boldsymbol{f} \in \mathbb{R}^{12}$, the object position in the (X_h, Z_h)-plane $\boldsymbol{p}_{m,xz} \in \mathbb{R}^2$, the prismatic joints $\boldsymbol{q}_s := [q_{11}\ q_{21}]^{\mathrm{T}}$ and the contact points ${}^m\boldsymbol{p}_c \in \mathbb{R}^{12}$. The force and position vectors are expressed in the hand frame Σ_h. The optimization is formulated as

$$\max_{f\in\mathcal{F}, p_{m,xz}\in\mathcal{P}_{m,xz}, q_s\in\mathcal{Q}_s, {}^mp_c\in\mathcal{P}_c} V(\boldsymbol{f}, \boldsymbol{p}_{m,xz}, \boldsymbol{q}_s, {}^m\boldsymbol{p}_c), \tag{24}$$

where V is an optimization criterion and $\mathcal{F}$, $\mathcal{P}_{m,xz}$, $\mathcal{Q}_s$ and $\mathcal{P}_c$ are constraint sets. In the latter, these are shown. *Note that the optimization problem (24) is considered in the 3D situation although the (x, z) components of the object position are only optimized. This is because the contact points on the object is not restricted in 2D space.*

3.2 Constraint Sets

Equilibrium of Forces The grasping forces are balanced with the gravity force:

$$\sum_{i=0}^{3} \boldsymbol{f}_i + m\boldsymbol{g} = \boldsymbol{0}, \quad \sum_{i=0}^{3} \boldsymbol{p}_i \times \boldsymbol{f}_i + \boldsymbol{p}_m \times m\boldsymbol{g} = \boldsymbol{0}, \tag{25}$$

where m is the mass of the object and $\boldsymbol{g} \in \mathbb{R}^3$ is the gravity vector. (25) is transformed to the linear matrix form:

$$\boldsymbol{A}_e \boldsymbol{f} = \boldsymbol{b}_e, \tag{26}$$

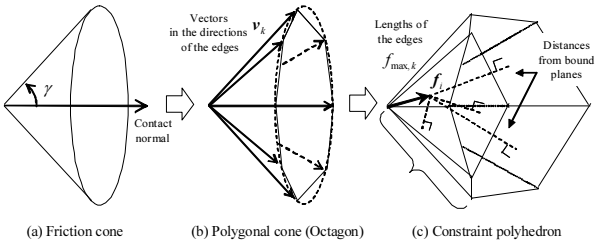

Fig. 11. A friction cone and its approximation.

where

$$\boldsymbol{A}_e := \left[\boldsymbol{G}(\boldsymbol{p}_0)\ \cdots\ \boldsymbol{G}(\boldsymbol{p}_3)\right],\ \boldsymbol{b}_e := -\boldsymbol{G}(\boldsymbol{p}_m)m\boldsymbol{g}$$

$$\boldsymbol{G}(\boldsymbol{x}) := \left[\boldsymbol{I}_3\ \ \boldsymbol{S}(\boldsymbol{x})^{\mathrm{T}}\right]^{\mathrm{T}},\ \boldsymbol{S}(\boldsymbol{x})\boldsymbol{y} := \boldsymbol{x} \times \boldsymbol{y}.$$

Note that $\boldsymbol{S}(\boldsymbol{x}) \in \mathbb{R}^{3\times3}$ is the skew-symmetric matrix to be equivalent to the cross product of $\boldsymbol{x}$.

Friction and Torque Limitations Figure 11 illustrates a friction cone. The friction cone is defined as

$$|\boldsymbol{t}_{x_i}^{\mathrm{T}} \boldsymbol{f}_i| \le \mu \boldsymbol{n}_i^{\mathrm{T}} \boldsymbol{f}_i,\ |\boldsymbol{t}_{y_i}^{\mathrm{T}} \boldsymbol{f}_i| \le \mu \boldsymbol{n}_i^{\mathrm{T}} \boldsymbol{f}_i, \tag{27}$$

where $\boldsymbol{t}_{x_i}, \boldsymbol{t}_{y_i} \in \mathbb{R}^3$ are the tangent vectors, $\boldsymbol{t}_{x_i}^{\mathrm{T}} \boldsymbol{t}_{y_i} = 0$ and μ is the friction coefficient between the finger and object. Note that the angle γ in the figure (a) is defined as $\gamma := \tan^{-1}\mu$. The cone is approximated to a polygonal cone to touch to the cone internally as in the figure (b), which is an example of an octagonal cone. $\boldsymbol{v}_k$ is the unit vector in the direction of the kth edge of the cone. The force limitation can be considered by obtaining the maximum force $f_{\max,k}$ in the direction of $\boldsymbol{v}_k$ using Theorem 3. Therefore, the cone in the figure (b) is modified to the *constraint polyhedron.* Note that the lengths of the edges of $\boldsymbol{v}_k$ of the polyhedron. The constraint polyhedron of ith force is formulated as

$$\boldsymbol{A}_{f_i} \boldsymbol{f}_i \le \boldsymbol{b}_{f_i}, \tag{28}$$

where $\boldsymbol{A}_{f_i} \in \mathbb{R}^{(K+N_K)\times3}$, $\boldsymbol{b}_{f_i} \in \mathbb{R}^{(K+N_K)}$, $N_K := {}_K C_3$ and K is the number of the apexes the polygon of the approximated cone. The first K numbers of the inequalities mean that the force is inside the approximated cone and the second N_K numbers of the inequalities mean that the force satisfies the force limitation.

Example 2. Figure 12 shows an example of an approximated friction cone. The all joints are 0 and the contact normal $\boldsymbol{n} = [0\ 0\ -1]^{\mathrm{T}}$. The friction coefficient is $\mu = 2.86$

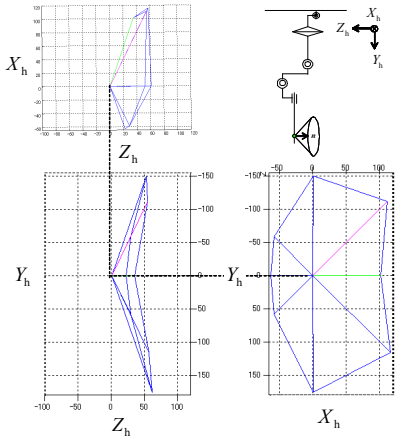

Fig. 12. An example of an approximated friction cone.

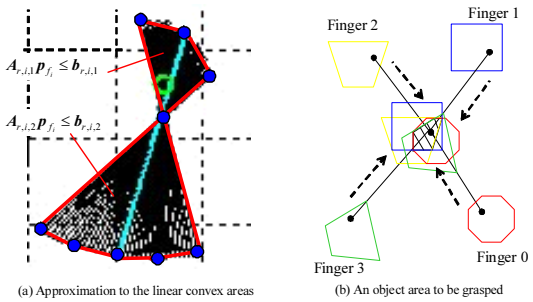

(a) Approximation to the linear convex areas (b) An object area to be grasped

Fig. 13. Approximation of the reachable area of the finger.

of the one between the urethane and the mirror. The figures are plotted in the hand frame Σ_h. It is confirmed that the friction cone is modified to the polyhedron.

Constrained Area of Object Position The reachable areas of the fingers are depicted by Theorem 1 with given the contact points and normal vectors as in Fig. 9 of the example 1. The coordinates on the bounds of the reachable areas in the (X_h, Z_h)-plane are given by (3) and (4). Therefore, the reachable area in the (X_h, Z_h)-plane of the finger is approximated to some linear convex areas as shown in Fig. 13 (a):

$$\boldsymbol{A}_{r,i,\alpha_i}\boldsymbol{p}_{c_i,xz} \leq \boldsymbol{b}_{r,i,\alpha_i},\ \alpha_i = 1,\ 2, \cdots, \tag{29}$$

where $\boldsymbol{p}_{c_i,xz} \in \mathbb{R}^2$ is the contact position in the (X_h, Z_h)-plane and α_i is the number of the independent convex areas. In the cases of the fingers 0 and 1, (29) is modified as

$$\boldsymbol{A}_{r,i,\alpha_i}(\boldsymbol{p}_{c_i,xz} - [0\ \ q_{i1}]^{\mathrm{T}}) \leq \boldsymbol{b}_{r,i,\alpha_i},\ \alpha_i = 1,\ 2, \cdots. \tag{30}$$

The object area for the finger i to reach at the contact point $\boldsymbol{p}_{c_i,xz}$ is easily calculated by (23) as

$$\begin{aligned} &\boldsymbol{A}_{r,i,\alpha_i}(\boldsymbol{p}_{m,xz} + \boldsymbol{p}_{mc_i,xz}) \leq \boldsymbol{b}_{r,i,\alpha_i} \\ \Leftrightarrow &\boldsymbol{A}_{r,i,\alpha_i}\boldsymbol{p}_{m,xz} \leq \boldsymbol{b}_{r,i,\alpha_i} - \boldsymbol{A}_{r,i,\alpha_i}\boldsymbol{p}_{mc_i,xz}, \end{aligned} \tag{31}$$

where $\boldsymbol{p}_{mc_i,xz} \in \mathbb{R}^2$ is the x and z components of $\boldsymbol{R}_m\,{}^m\boldsymbol{p}_{c_i}$. (30) is also transformed to the similar form. Note that (29) and (30) are moved in parallel to areas around the center of mass as in the figure (b). Considering the product sets between (29) and (30) with respect to the number i as illustrated in the figure (b), we obtain the object areas for all the fingers to reach at the contact points:

$$\boldsymbol{A}_{m,\beta}\boldsymbol{x} \leq \boldsymbol{b}_{m,\beta},\ \beta = 1,\ 2, \cdots, \tag{32}$$

where

$$\boldsymbol{x} := \begin{bmatrix} \boldsymbol{p}_{m,xz}^{\mathrm{T}} & \boldsymbol{q}_s^{\mathrm{T}} \end{bmatrix}^{\mathrm{T}} \in \mathbb{R}^4$$

and β is the number of the product sets of (31).

Searching Areas of Contact Points Suppose the discrete contact points on the object are given. The searching area of the ith contact point ${}^m\boldsymbol{p}_{c_i}$ is the circle with the origin ${}^m\boldsymbol{p}_{c_i}$:

$$\mathcal{P}_{c_i} = \{\boldsymbol{p} \mid \boldsymbol{p} \in \mathcal{C},\ \|\boldsymbol{p} - \boldsymbol{p}_{c_i}\| \leq r_{c_i}\}, \tag{33}$$

where $\mathcal{C}$ is the set of the points on the object.

3.3 Optimization Criterion

The distances of the grasping force $\boldsymbol{f}_i$ from the constraint polyhedron are considered as the optimization criterion as shown in Fig. 11 (c). The distances are calculated as

$$d_{il} := \|\boldsymbol{a}_{f_l}\|^{-1}\widehat{d}_{il}, \tag{34}$$

where $\boldsymbol{a}_{f_l} \in \mathbb{R}^{1\times 2}$ is the lth row vector of $\boldsymbol{A}_{f_i}$ and d_{il} is the lth component of

$$\widehat{\boldsymbol{d}}_i := \boldsymbol{b}_{f_i} - \boldsymbol{A}_{f_i}\boldsymbol{f}_i \tag{35}$$

$\|\boldsymbol{a}_{f_l}\|^{-1}$ is the scaling operator and d_{il} is the distance of the grasping force $\boldsymbol{f}_i$ from the boundary plane of the finger i. The optimization criterion V is defined as

$$V := \min_{i,l} d_{il}. \tag{36}$$

Suppose that the optimized value of V is $d_{\min}$. Let us consider the allowable disturbance force from $d_{\min}$. From (26), the force equilibrium with the disturbance $\boldsymbol{f}_d$ is given by

$$\boldsymbol{A}_e(\boldsymbol{f} + \delta\boldsymbol{f}) = \boldsymbol{b}_e - \boldsymbol{G}(\boldsymbol{p}_m)\boldsymbol{f}_d, \tag{37}$$

where $\delta\boldsymbol{f} \in \mathbb{R}^{12}$ denotes the grasping forces to balance to $\boldsymbol{f}_d$. Substituting (26) into (37) leads to

$$\boldsymbol{A}_e\delta\boldsymbol{f} = -\boldsymbol{G}(\boldsymbol{p}_m)\boldsymbol{f}_d. \tag{38}$$

Solving (38) with respect to $\boldsymbol{f}_d$ results in

$$\boldsymbol{f}_d = -\boldsymbol{G}(\boldsymbol{p}_m)^+\boldsymbol{A}_e\delta\boldsymbol{f}, \tag{39}$$

where $\boldsymbol{G}^+$ is the pseudo matrix of $\boldsymbol{G}$. With the singular value decomposition of $\boldsymbol{G}(\boldsymbol{p}_m)^+\boldsymbol{A}_e$ (39) is rewritten as

$$\boldsymbol{f}_d = -\boldsymbol{U}\begin{bmatrix}\boldsymbol{\Sigma} & \boldsymbol{0}_{3\times 9}\end{bmatrix}\boldsymbol{V}^{\mathrm{T}}\delta\boldsymbol{f}, \tag{40}$$

where $\boldsymbol{U} \in \mathbb{R}^{3\times 3}$, $\boldsymbol{V} \in \mathbb{R}^{12\times 12}$ and

$$\boldsymbol{\Sigma} = \begin{bmatrix}\sigma_1 & & 0 \\ & \sigma_2 & \\ 0 & & \sigma_3\end{bmatrix}.$$

Since $\delta\boldsymbol{f}$ represents the allowable forces, $\delta\boldsymbol{f}$ can be expressed as

$$\delta\boldsymbol{f} = d_{\min}\boldsymbol{e},\ \|\boldsymbol{e}\| = 1, \tag{41}$$

where $\boldsymbol{e} \in \mathbb{R}^{12}$ is an arbitrary vector. Substituting (41) into (40), we get

$$\boldsymbol{f}_d = -\boldsymbol{U}\begin{bmatrix} d_{\min}\sigma_1 & & 0 \\ & d_{\min}\sigma_2 & \\ 0 & & d_{\min}\sigma_3 \end{bmatrix}\boldsymbol{e}_{v_1}, \tag{42}$$

where $[\boldsymbol{e}_{v_1}^{\mathrm{T}}\ \boldsymbol{e}_{v_2}^{\mathrm{T}}]^{\mathrm{T}} := \boldsymbol{V}^{\mathrm{T}}\boldsymbol{e}$, $\boldsymbol{e}_{v_1} \in \mathbb{R}^3$ and $\boldsymbol{e}_{v_2} \in \mathbb{R}^9$. Therefore, $\boldsymbol{f}_d$ is represented as the ellipsoid with the main axes of the colums in $\boldsymbol{U}$ and the sizes of $(d_{\min}\sigma_1, d_{\min}\sigma_2, d_{\min}\sigma_3)$ in the major axes. The allowable magnitude of $\boldsymbol{f}_d$ is given by

$$\xi := \min(d_{\min}\sigma_1, d_{\min}\sigma_2, d_{\min}\sigma_3). \tag{43}$$

3.4 Optimization Problem

The problem (24) is considered by the following two separated problems:

$$\max_{p_{m,xz}\in\mathcal{P}_m, x\in\mathcal{X}} \max_{f\in\mathcal{F}} V(\boldsymbol{f}, \boldsymbol{p}_{m,xz}, \boldsymbol{q}_s; {}^m\boldsymbol{p}_c) \tag{44}$$

$$\max_{{}^m p_c\in\mathcal{P}} \max_{f\in\mathcal{F}} V(\boldsymbol{f}, {}^m\boldsymbol{p}_c; \boldsymbol{p}_{m,xz}, \boldsymbol{q}_s). \tag{45}$$

These problems are solved by turns and iteratively.

Example 3. The initial contact points and normal vectors are

$$\boldsymbol{p}_A = \begin{bmatrix}76\\-31\\27\end{bmatrix},\ \boldsymbol{p}_B = \begin{bmatrix}-72\\-37\\27\end{bmatrix},\ \boldsymbol{p}_C = \begin{bmatrix}-52\\-28\\-49\end{bmatrix},\ \boldsymbol{p}_D = \begin{bmatrix}53\\-24\\-49\end{bmatrix}$$

$$\boldsymbol{n}_A = \begin{bmatrix}-0.99\\0.02\\0.12\end{bmatrix}, \boldsymbol{n}_B = \begin{bmatrix}0.99\\0.06\\0.01\end{bmatrix}, \boldsymbol{n}_C = \begin{bmatrix}0.44\\0.11\\0.89\end{bmatrix}, \boldsymbol{n}_D = \begin{bmatrix}-0.75\\0.01\\0.66\end{bmatrix}.$$

The configuration of the contact points are similar to Fig. 8. The initial 1st joints of the fingers 0, 1 are

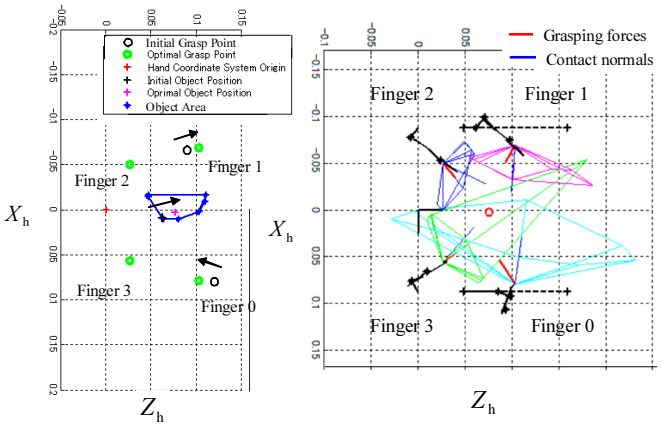

Fig. 14. The optimization result of the grasp of the mirror.

$\boldsymbol{q}_s = [0 \quad 0]^{\mathrm{T}}$ [mm]. The initial object position is $\boldsymbol{p}_{m,xz} = [10 \quad 63]^{\mathrm{T}}$ [mm]. The grasping forces are optimized by the initial values as

$$\boldsymbol{f}_0 = \begin{bmatrix} -5.6 \\ -3.7 \\ -2.1 \end{bmatrix}, \ \boldsymbol{f}_1 = \begin{bmatrix} 10 \\ -11 \\ -8.9 \end{bmatrix}, \ \boldsymbol{f}_2 = \begin{bmatrix} 1 \\ 0.80 \\ 6.7 \end{bmatrix}, \ \boldsymbol{f}_3 = \begin{bmatrix} -5.6 \\ -8.9 \\ -4.3 \end{bmatrix}$$

and the allowable disturbance is $\xi = 7.1$ [N]. The optimal values of the 1st joints and the object position are $\boldsymbol{q}_s = [36 \quad 13]$ and $\boldsymbol{p}_{m,xz} = [-2.8 \quad 76]$ [mm]. The values of the grasping forces are

$$\boldsymbol{f}_0 = \begin{bmatrix} -20 \\ -8.1 \\ -13 \end{bmatrix}, \ \boldsymbol{f}_1 = \begin{bmatrix} 15 \\ -6.6 \\ -8.5 \end{bmatrix}, \ \boldsymbol{f}_2 = \begin{bmatrix} 13 \\ -5.4 \\ 11 \end{bmatrix}, \ \boldsymbol{f}_3 = \begin{bmatrix} -7.4 \\ -2.6 \\ -10.4 \end{bmatrix}.$$

It is confirmed that the internal forces become stronger because the magnitudes of the z components of the grasping forces. The optimization result is shown in Fig. 14. The left figure shows the initial and optimal contact points and object position and the object area. As for the object position, the black cross of the initial point moves to the purple cross of the inner optimal point in the blue object area. As for the contact points, the black circles of the initial points of the finger 0 and 1 moved to the green circles of the optimal points. It is confirmed that the symmetry of the configuration of the optimal contact points is better than that of the initial contact points. The right figure illustrates the grasping forces and friction cones. The red lines of the grasping forces are close to the blue lines of the contact normals. The allowable magnitude of the disturbance is optimized from $\xi = 7.1$ to $\xi = 22$ [N]. Furthermore, $d_{\min}\sigma_1$, $d_{\min}\sigma_2$ and $d_{\min}\sigma_3$ are almost same. This means that the ellipsoid of $\boldsymbol{f}_d$ is approximated to the sphere with the radius ξ by the optimization.

4. CONTROL METHOD

The grasping forces are realized by a position-based controller (e.g., See Murakami et al. (1993)). In view of fault tolerance in product lines, the forces should be controlled without any force sensors. Then, a control method is shown briefly, which consists of a force estimation and a force controller.

The static relation of (18) with the effect of the joint friction is given by

$$\boldsymbol{\tau} \pm \boldsymbol{\tau}_f = \boldsymbol{J}^{\mathrm{T}} \boldsymbol{f}, \tag{46}$$

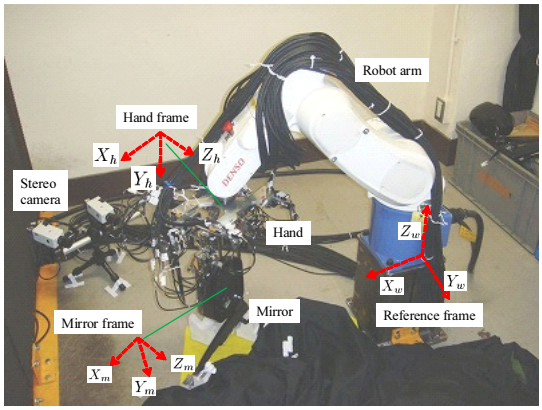

Fig. 15. Overview of the experimental environment.

where $\boldsymbol{\tau}_f \in \mathbb{R}^4$ is the joint friction. Solving (46) yields

$$\boldsymbol{f} = (\boldsymbol{J}^{\mathrm{T}})^{+}(\boldsymbol{\tau} + \boldsymbol{\tau}_f), \tag{47}$$

where $(\boldsymbol{J}^{\mathrm{T}})^{+} \in \mathbb{R}^{3\times 4}$ is the pseudo inverse matirx of $\boldsymbol{J}^{\mathrm{T}}$. τ_{f_i} is defined as

$$\tau_{f_i} \in \Upsilon_i, \ \Upsilon_i := \{\tau \mid -\tau_{f_{m_i}} \le \tau \le \tau_{f_{p_i}}\}, \tag{48}$$

where $\tau_{f_{m_i}}$ and $\tau_{f_{p_i}}$ are the maximum friction in the positive and negative directions of the joints. Note that it is impossible to determine the frictions generated at the joints because the static frictions of the joints are *hyperstatic*. Therefore, we use the mean value of (47) as the estimated grasping force.

The force controller consists of the following two parts:

$$\boldsymbol{\tau} = -\boldsymbol{K}_p(\boldsymbol{q} - \boldsymbol{q}_d) - \boldsymbol{K}_v(\dot{\boldsymbol{q}} - \dot{\boldsymbol{q}}_d) - \boldsymbol{K}_i \int (\boldsymbol{q} - \boldsymbol{q}_d)dt \tag{49}$$

$$\boldsymbol{q}_d := \boldsymbol{g}(\boldsymbol{p}_d), \ \boldsymbol{p}_d := \boldsymbol{p}_0 + \Delta\boldsymbol{p}_d \tag{50}$$

$$\Delta\boldsymbol{p}_d := -\boldsymbol{K}_{f_p}(\boldsymbol{f} - \boldsymbol{f}_d) - \boldsymbol{K}_{f_i} \int (\boldsymbol{f} - \boldsymbol{f}_d)dt,$$

where $\boldsymbol{q}_d \in \mathbb{R}^4$ and $\boldsymbol{f}_d \in \mathbb{R}^3$ are the references of the joint angles and grasping forces and $\boldsymbol{p}_0 \in \mathbb{R}^3$ is the fingertip position when the fingers contact on the object. Note that the subscript i is dropped here for simple notation. $\boldsymbol{K}_*$ is the positive definite matrix of the control gain. $\boldsymbol{q} : \mathbb{R}^3 \to \mathbb{R}^4$ represents the inverse kinematics with the constraint $q_3 + q_4 = Q_{34}(q_2^0)$, where q_2^0 is the 2nd joint angle in initial contact situation. $\Delta\boldsymbol{p}_d \in \mathbb{R}^3$ is the reference variation of $\boldsymbol{p}_d$ due to the force error.

5. EXPERIMENT

Figure 15 shows the overview of the experimental environment. The hand is attached to the robot arm (VS-6556G, DENSO Co. Ltd.). The reference frame Σ_w is set to the base of the arm. The position and orientation of the hand with respect to Σ_w, $({}^w\boldsymbol{p}_h, \boldsymbol{R}_{wh})$, are related to $({}^h\boldsymbol{p}_m, \boldsymbol{R}_{hm})$ with respect to Σ_h by

$${}^w\boldsymbol{p}_m = {}^w\boldsymbol{p}_h + \boldsymbol{R}_{wh}{}^h\boldsymbol{p}_m, \ \boldsymbol{R}_{wm} = \boldsymbol{R}_{mh}\boldsymbol{R}_{hm}, \tag{51}$$

where $({}^w\boldsymbol{p}, \boldsymbol{R}_{wm})$ are preliminarly set and $({}^h\boldsymbol{p}_m, \boldsymbol{R}_{hm})$ are the optimized values. The arm is used for adjusting $({}^w\boldsymbol{p}_h, \boldsymbol{R}_{wh})$ to the values calculated by (51). The mirror is supported by a seat in order to be similar orientation as in Fig. 8. The orientation of the hand is also moved over the mirror in order to be similar orientation as in Fig. 8. The position and orientation is calculated by the feature

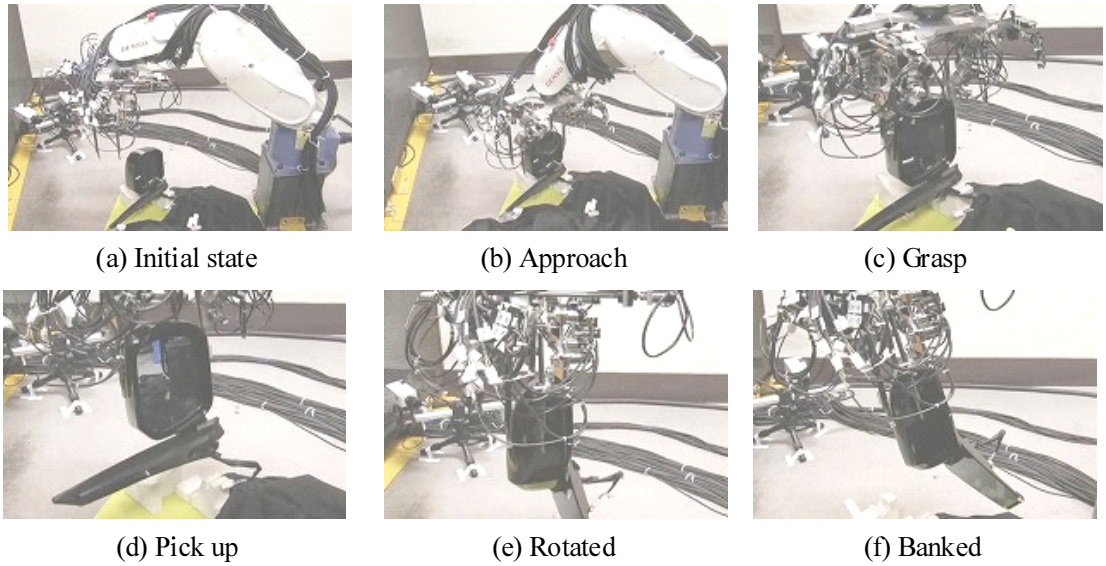

(a) Initial state (b) Approach (c) Grasp

(d) Pick up (e) Rotated (f) Banked

Fig. 16. Snapshots of the experiment of the grasp of the mirror.

points on the mirror detected by the stereo camera. The optimal values are same as in Example 3.

Figure 16 shows snapshots of the experiment of the grasp of the mirror. The hand is at the initial position in the figure (a) approaches the mirror by the arm in the figure (b). The fingers contact on and grasp the mirror in the figure (c). After 10 [s] for the converge of the controlled grasping forces, the mirror is picked up by the hand and arm in the figure (d). The grasped mirror is rotated and banked as in the figure (e) and (f), which show the effectiveness of the proposed grasp optimization.

6. CONCLUSIONS

This paper proposed the synthesis methodology of stable grasp by the four-fingered robot hand in order to automate the preparation for assembling work. The optimization method of the grasping forces, the object configuration and the contact points was proposed. The criterion of the optimization was the appropriate normalized distances from the planes of the constraint polyhedron, which is derived by the friction and joint torque limitations. The experimental result of the grasp of the door mirror was shown to verify the effectiveness the proposed method.

In our optimization method, the y coordinate of the object position and the object orientation have not been considered. Integrating these degrees of freedom can improve the optimization method. Furthermore, it is necessary to verify the grasp of another variety shaped object.

REFERENCES

Kerr, J. and Roth, B. (1986). Analysis of multifingered robot hands. *Int. J. Robot. Res.*, 4(4), 3–17.

Li, Y., Yu, Y., and Tsujio, S. (2002). An analytical grasp planning on given object with multifingered hand. In *Proc. IEEE Int. Conf. Robot. Automat.*, 3749–3754.

Li, Z. and Sastry, S.S. (1988). Task-oriented optimal grasping by multifingered robot hands. *IEEE J. Robot. Automat.*, 4(1), 32–44.

Magialardi, L., Mantriota, G., and Trentadue, A. (1996). A three-dimensional criterion for the determination of optimal grip points. *Robot. Computer-Integrated Man.*, 12(2), 157–167.

Markenscoff, X. and Papadimitriou, C.H. (1989). Optimum grip of a polygon. *Int. J. Robot. Res.*, 8(2), 17–29.

Murakami, T., Oda, N., Miyasaka, Y., and Ohnishi, K. (1993). Force sensorless impedance control by disturbance observer. In *Proc. of Power Conv. Conf.*, 352–357.

Nakamura, Y., Nagai, K., and Yoshikawa, T. (1989). Dynamics and stability in coordination of multiple robotic mechanisms. *Int. J. Robot. Res.*, 8(2), 44–61.

Nguyen, V. (1988). Constructing force-closure grasps. *Int. J. Robot. Res.*, 7(3), 3–16.

Omata, T. (1990). Fingertip positions of a multifingered hand. In *Proc. IEEE Int. Conf. Robot. Automat.*, 1562–1567.

Omata, T. (1993). Finger position computation for 3-dimentional equilibrium grasp. In *Proc. IEEE Int. Conf. Robot. Automat.*, 216–222.

Salisbury, J.K. and Roth, B. (1983). Kinematic and force analysis of articulated hands. *ASME J. Mech., Transmissions, Automat.*, 105(1), 35–41.

Trinkle, J.C. and Paul, R.P. (1990). Planning for dexterous manipulation with sliding contacts. *Int. J. Robot. Res.*, 9(3), 24–48.

Watanabe, T. and Yoshikawa, T. (2003a). Optimization of grasping an object by using required acceleration and equilibrium-force sets. In *Proc. IEEE/ASME Int. Conf. Adv. Intel. Mech.*, 338–343.

Watanabe, T. and Yoshikawa, T. (2003b). Optimization of grasping by using a required external force set. In *Proc. IEEE Int. Conf. Robot. Automat.*, 1127–1132.

Yoshikawa, T. and Nagai, K. (1991). Manipulating and grasping forces in manipulation by multifingered robot hands. *IEEE Trans. Robot. Automat.*, 7(1), 67–77.